Numerical Analysis of Three-Dimensional Magneto hybridized Nanofluid (Al_2O_3-Cu/H_2O) Radiative Stretchable rotating Flow with Suction

Bhavanam Naga Lakshmi
Department of Engineering Mathematics, Koneru Lakshmaiah Education Foundation, Guntur, Andhra Pradesh-522302, India
hemaevuri29@gmail.com (corresponding author)

V. S. Bhagavan
Department of Engineering Mathematics, Koneru Lakshmaiah Education Foundation, Guntur, Andhra Pradesh-522302, India
drvsb002@kluniversity.in

Ravuri Mohana Ramana
Department of Mathematics, Narasaraopeta Engineering College (Autonomous), Narasaraopet, Andhra Pradesh, India
mohanaramanacrypto@gmail.com

Chundru Maheswari
Department of Mathematics, Narasaraopeta Engineering College (Autonomous), Narasaraopet, Andhra Pradesh, India
cmaheswari2014@gmail.com

Received: 20 June 2024 | Revised: 11 July 2024 | Accepted: 19 July 2024

 DOI: https://doi.org/10.48084/etasr.8183

ABSTRACT

The current study aims to investigate the heat generation/absorption, radiation, and chemical reaction impacts on a laminar flow, with an upward half-space three-dimensional, incompressible permeable, stretchable, rotating hybrid nanofluid (Al_2O_3-Cu/H_2O). Using appropriate similarity transformations, leading nonlinear governing equations were taken into account and were converted into ordinary differential equations. These equations were evaluated by deploying MATLAB's bvp5c feature. The resulting graphs assess velocity, temperature, and concentration for a range of effects. Additionally, Sherwood and Nusselt numbers and skin friction results were obtained. The findings were compared with previously published research.

Keywords-hybrid nanofluid; magnetic field; rotational stretching sheet; suction; heat source; chemical reaction

I. INTRODUCTION

Nanofluids have superior thermal characteristics compared to their base fluids and outperform them in heat transfer applications. They are primarily employed in industries to produce thermal power, chemical reactions, heat production, transportation, etc. Using Hybrid Nanofluids (HNFs), researchers have recently sought to increase heat transfer rates. HNFs have more than one type of nanoparticles mixed with a base fluid. They additionally have more favorable thermal properties than conventional base fluids and nanofluids. Authors in [1] presented a synthesis of a hybrid nanofluid of Al-Cu nanoparticles with water as the base fluid, in a two-step procedure and their thermophysical characteristics. Authors in [2] scrutinized developments in heat transfer on HNF. Fluids with good electrical conductivity in a magnetic field are the focus of MHD research. Numerous applications, including flow measurement, nuclear waste disposal, polymer sheet extraction,

hot rolling, etc., use this idea. The investigation of the various impacts of MHD HNF was performed via a stretching sheet. Authors in [3, 4] analyzed numerically the 3-dimensional HNF Al_2O_3-Cu/H_2O flow past a stretched wall subject to Newtonian heating with effecting Lorentz force, and the flow passing through a stretching sheet with suction. Authors in [5] investigated the enhancement of heat transfer of Cu-Al_2O_3/water HNF stretched wall flow. According to [6], exponential stretching and contracting of the sheet causes magnetized heat to transfer rotational flow of the ferrofluid. Authors in [7] proposed an exponential stretched wall, on HNF heat transfer and stagnation point flow with slip velocity effect. Heat transfer of HNF transient flow past a shirked wall along a permeable, nonlinear permeable surface, was identified in [8-10]. Authors in [11] demonstrated a magneto HNF axisymmetric radially permeable shrinking wall with ohmic heating.

Thermal radiation is electromagnetic radiation that comes from the movement of the matter's particles. A crucial role is played by the heat transfer in different flows when thermal radiation is present. Magneto heat transfer of the axisymmetric flow of HNFs through a permeable radiative stretched wall with ohmic heating on a nonlinearly stretching wall with a radiation effect was observed in [12]. Joule heating on a nonlinearly radiative stretching regime was evideenced on HNF magneto axisymmetric flow past a permeable regime. The HNF's magnetized rotating flow along with its radiation impacts was studied in [13]. Authors in [14] scrutinized the 3-dimensional HNF magnetized rotating flow with the thermal radiation effect. Furthermore, in [15], a rotating HNF combined a stretched wall with an erratic 3-D flow. Authors in [16] made theoretical arguments in favor of a 3-D magnetized HNF source-sink past a stretched regime. A hybrid radiative ferrofluid over a porous shrinking wall was investigated in 3-D, in [17]. In [18], a numerical analysis was carried out on the convective heat transfer of Al_2O_3/Water-Ethylene Glycol (W-EG) and CuO/(W-EG) nanofluids moving through a circular tube with circumferentially non-uniform heating under laminar flow conditions. The discussion performed in [19] focuses on a rotating, stretched wall over a nanofluid with radiation and suction impacts. Authors in [20, 21] compared flow and heat transfer enhancement properties between a spinning nanofluid and a hybrid nanofluid with velocity slip and thermal slip. Authors in [22] investigated numerically the MHD forchheimer flow of Fe_3O_4–H_2O, Cu–H_2O, and Ag–H_2O nanofluids over a permeable stretching sheet with radiation. Authors in [23] observed the effect of nanoparticle volume fraction on MHD water-based nanofluid flows over a permeable stretching sheet with suction/injection. Authors in [24] discussed multiple slips and heat source effects on the MHD stagnation point flow of the Casson fluid over a stretching sheet in the presence of a chemical reaction. The radiation and slip impacts of heat transfer of Fe_2O_3 and Fe-water base nanofluids across a porous stretching and shrinking sheet on the boundary layer flow were explored in [25]. Authors in [26] proposed a 3-D MHD hybrid nanofluid flow, by using Tiwari Das modal rotating stretched wall with Joule heating.

As far as is known, there is no literature available on radiation, heat generation, and chemical reaction impacts on sheets that are linearly suction stretched. The current study used MHD HNF Al_2O_3-Cu/H_2O to analyze the chemical reactions and the radiation impact over a stretched wall considering the literature. The bvp5c MATLAB solver was utilized to solve the governing equation system, which has been similarity transfigured into a non-linear ordinary differential equation. The novelty of this study is that it looks at a linearly stretching sheet under suction interacting with a magnetic field (M), a chemical reaction (R_c), heat generation (δ), and radiation (R). Additionally, studies on heat generation, radiation, chemical reactions, nanoparticle volume fraction, magnetic field, Schmidt number, and suction impact are carried out. The current article addresses significant knowledge gaps by investigating the complex interplay of multiple factors in fluid dynamics, such as the combined impacts of hybrid nanoparticles, magnetic fields, and intricate Boundary Conditions (BCs) like suction, rotation, and stretching. While existing studies often focus on simpler models or single component nanofluids, this work explores the behavior and advantages of HNFs in enhancing fluid flow and heat transfer properties. Additionally, the study examines the effects of magnetic fields and radiative heat transfer in three-dimensional flows, providing a more realistic portrayal of real-world scenarios. Overall, the research offers valuable insights for industrial and engineering applications, particularly in fields requiring efficient heating and cooling solutions.

II. METHODOLOGY

A. Mathematical Modeling

In this section the 3-dimensional Al_2O_3-Cu/H_2O MHD HNF flow over a permeable rotated stretched sheet with heat transfer is considered. It is incompressible, steady, Newtonian and laminar, occupying upward half space at $z \geq 0$. The assumptions are:

- HNF Al_2O_3-Cu/H_2O stretching in the x-direction, with velocity $U_w = ax$, is assumed.
- Vertical z axis with a constant velocity Ω, perpendicular to the wall is assessed.
- The HNF is impacted by a magnetic regime in the a direction parallel to the strength.
- $T_w = T_0 x^2$, refers to the temperature at the stretching regime, where T_0 refers to the characteristic temperature and T_∞ to the ambient temperature.

The governing equations such as the equation of continuity and the momentum along the x and y axes are taken from [26], while new heat source/sink effects and thermal radiation effects in energy equation are incorporated. Additionally, the concentration equation with thermos diffusion and chemical reaction impacts is considered.

$$\frac{\partial u}{\partial x}+\frac{\partial v}{\partial y}+\frac{\partial w}{\partial z}=0 \quad (1)$$

$$u\frac{\partial u}{\partial x}+v\frac{\partial u}{\partial y}+w\frac{\partial u}{\partial z}-2\Omega v=\frac{\mu_{hnf}}{\rho_{hnf}}\frac{\partial^2 u}{\partial z^2}-\frac{\sigma_{hnf}}{\rho_{hnf}}B^2 u \quad (2)$$

$$u\frac{\partial v}{\partial x}+v\frac{\partial v}{\partial y}+w\frac{\partial v}{\partial z}+2\Omega v=\frac{\mu_{hnf}}{\rho_{hnf}}\frac{\partial^2 v}{\partial z^2}-\frac{\sigma_{hnf}}{\rho_{hnf}}B^2 v \quad (3)$$

$$u\frac{\partial T}{\partial x}+v\frac{\partial T}{\partial y}+w\frac{\partial T}{\partial z}=\frac{k_{hnf}}{(\rho_{cp})_{hnf}}\frac{\partial^2 T}{\partial z^2}$$
$$-\frac{\sigma_{hnf}}{(\rho_{cp})_{hnf}}B^2(u^2+v^2)+\frac{Q}{(\rho_{cp})_{hnf}}(T-T_\infty)- \quad (4)$$
$$\frac{1}{(\rho_{cp})_{hnf}}\frac{\partial q_r}{\partial x}$$

$$u\frac{\partial c}{\partial x}+v\frac{\partial c}{\partial y}+w\frac{\partial c}{\partial z}=\beta_{hnf}\frac{\partial^2 c}{\partial z^2}-\xi_1(c-c_\infty)^n \quad (5)$$

where q_r is the radiation flux defined by:

$$q_r=\frac{-4\sigma}{3\chi}\frac{\partial T^4}{\partial z}$$

where σ and χ are the Stefan–Boltzman constant and the mean absorption coefficient, respectively.

Developing the Tailor series of T_∞, we have:

$$T^4 \cong 4TT^3\text{-}3T_\infty{}^4$$

with the following BCs:

$$u=\lambda U_w,\ v=0,\ w=w_w,\ T=T_w=T_0x^2+T_\infty,\ \text{as } z=0 \quad (6)$$

$$u\to 0, v\to 0, T\to T_\infty \quad \text{as} \quad z\to\infty \quad (7)$$

By using the above BC [21, 22], similarity transformations turned the system of PDEs [1-5] into a system of ODEs:

$$w=-\sqrt{a\upsilon_f}\,f(\eta),\quad v=ayg(\eta),\quad u=axf'(\eta),$$
$$\theta(\eta)=\frac{T-T_\infty}{T_w-T_\infty},\quad \phi(\eta)=\frac{c-c_\infty}{c_w-c_\infty},\quad \eta=z\sqrt{\frac{a}{\upsilon_f}} \quad (8)$$

where η is a similarity variable and a is a positive constant.

By using the similarity variables (5), (1)-(4) are transfigured as nonlinear ODEs:

$$f'''(\eta)-(1-\phi_1)^{2.5}(1-\phi_2)^{2.5}\left((1-\phi_2)\left\{(1-\phi_1)+\phi_1\left(\frac{\rho_{s1}}{\rho_f}\right)\right\}+\phi_2\left(\frac{\rho_{s2}}{\rho_f}\right)\right)\left(f'^2(\eta)-f(\eta)f''(\eta)-2\varepsilon g(\eta)+\left(\frac{\sigma_{hnf}}{\sigma_f}\right)Mf'(\eta)\right)=0 \quad (9)$$

$$g''(\eta)-(1-\phi_1)^{2.5}(1-\phi_2)^{2.5}\left((1-\phi_2)\left\{(1-\phi_1)+\phi_1\left(\frac{\rho_{s1}}{\rho_f}\right)\right\}+\phi_2\left(\frac{\rho_{s2}}{\rho_f}\right)\right)\left(f'(\eta)g(\eta)-f(\eta)g'(\eta)+2\varepsilon g(\eta)+\left(\frac{\sigma_{hnf}}{\sigma_f}\right)Mg(\eta)\right)=0 \quad (10)$$

$$\left(\frac{K_{hnf}}{K_f}+\frac{4R}{3}\right)\theta''(\eta)-\Pr\left((1-\phi_2)\left\{(1-\phi_1)+\phi_1\left(\frac{(\rho_{cp})_{s1}}{(\rho_{cp})_f}\right)\right\}+\phi_2\left(\frac{(\rho_{cp})_{s1}}{(\rho_{cp})_f}\right)\right)\left(\left(2f'(\eta)\theta(\eta)-f(\eta)\theta'(\eta)\right)-\left(\frac{\sigma_{hnf}}{\sigma_f}\right)M\left(f'^2(\eta)+g^2(\eta)\right)-\delta\theta(\eta)\right)=0 \quad (11)$$

$$\phi''(\eta)=\frac{Sc}{(1-\phi_1)(1-\phi_2)}\left(Rc\phi(\eta)-f(\eta)\phi'(\eta)\right) \quad (12)$$

This change in BCs is represented by:

$$f(0)=S,\ f'(0)=\lambda,\ g(0)=0,\ \theta(0)=1,\ \phi(0)=1 \quad \text{at} \quad \eta=0 \quad (13)$$

$$f'(\eta)\to 0,\ g(\eta)\to 0,\ \theta(\eta)\to 0,\ \phi(\eta)\to 0 \quad \text{as} \quad \eta\to\infty \quad (14)$$

The controlling factors are:

$$M=\frac{B^2\sigma_f}{a\rho_f},\ Ec=\frac{a^2}{T_0(c_p)_f},\ Pr=\frac{(\mu C_p)_f}{k_f},$$
$$\epsilon=\frac{\Omega}{a},\ \lambda=\frac{b}{a},\ R=\frac{4\sigma T^4}{\chi K_f},\ Sc=\frac{\nu_f}{\beta_f},$$
$$\delta=\frac{Q}{a(\rho C_p)_f},\ R_c=\frac{\xi_1(C-C_\infty)}{a} \quad (15)$$

where C_{fx} and C_{fy} are the skin friction coefficients towards the x and y axis, respectively Nu_x and Sh_x are the Nusselt number and the Sherwood number.

$$C_{fx}=\frac{\mu_{hnf}}{\rho_f(U_w)^2}\left(\frac{\partial u}{\partial z}\right)_{z=0},\ C_{fx}=\frac{\mu_{hnf}}{\rho_f(U_w)^2}\left(\frac{\partial v}{\partial z}\right)_{z=0},$$
$$Nu_x=\frac{-\chi K_{hnf}}{K_f(T_w-T_\infty)}\left(\frac{\partial T}{\partial z}\right)_{z=0}, \quad (16)$$
$$Sh_x=\frac{-\chi K_{hnf}}{K_f(C_w-C_\infty)}\left(\frac{\partial C}{\partial z}\right)_{z=0}$$

or:

$$\sqrt{Re_x}C_{fx}=\frac{\mu_{hnf}}{\mu_f}f''(0),\ \sqrt{Re_x}C_{fy}=\frac{\mu_{hnf}}{\mu_f}g'(0),$$

$$\frac{Nu_x}{\sqrt{Re_x}} = -\frac{K_{hnf}}{K_f}\theta'(0), \qquad (17)$$

$$Re^{-\frac{1}{2}} Sh_x = -\frac{K_{hnf}}{K_f}\phi'(0)$$

where $Re = \frac{U_w\, x}{\nu_f}$ is the restricted Reynolds number.

III. NUMERIC QUANTIFIABLE METHOD

The converted system of nonlinear ODE's (9)-(12) with BCs in (13)-(14) was solved numerically by the bvp5c MATLAB solver. The following procedures were followed to implement the bvp5c solver into the problem.

1. The system of higher order nonlinear ODEs receives new variables in (9)-(12):

$$y(1) = f, y(2) = f', y(3) = f'', y(4) = g,$$
$$y(5) = g', y(6) = \theta, y(7) = \theta' \qquad (18)$$

2. Make the higher order nonlinear ODEs (9)-(12) simpler:

$$f' = y(2),\ f'' = y(3),$$

$$f''' = \left(\begin{array}{l} \left(y(2)\right)^2 - y(1)y(3) - 2\Omega y(4) + \\ \frac{\sigma_{hnf}/\sigma_f}{\rho_{hnf}/\rho_f}.M.y(2) \end{array} \right) \frac{\rho_{hnf}/\rho_f}{\mu_{hnf}/\mu_f},$$

$$g' = y(5),$$

$$g'' = \left(\begin{array}{l} y(2)y(4) - y(1)y(5) \\ +2\Omega y(2) + \frac{\sigma_{hnf}/\sigma_f}{\rho_{hnf}/\rho_f}.M.y(4) \end{array} \right) \frac{\rho_{hnf}/\rho_f}{\mu_{hnf}/\mu_f},$$

$$\theta' = y(7), \qquad (19)$$

$$\theta'' = \left(\begin{array}{l} 2y(2)y(6) - y(1)y(7) - \frac{\sigma_{hnf}/\sigma_f}{\left(\rho_{cp}\right)_{hnf}/\left(\rho_{cp}\right)_f}. \\ M.Ec\left(\left(y(2)\right)^2 + \left(y(4)\right)^2\right) - \delta\theta \end{array} \right) \times$$

$$\frac{\Pr\left(\rho_{cp}\right)_{hnf}/\left(\rho_{cp}\right)_f}{\left(\frac{k_{hnf}}{k_f} + \frac{4}{3}R\right)},$$

$$\phi' = y(9),$$

$$\phi'' = \frac{Sc}{(1-\phi_1)(1-\phi_2)}\left(R_c\theta - f\theta'\right)$$

3. The BCs are:

$$y_a(1) = S,\ y_a(2) = \lambda,\ y_a(4) = 0,\ y_a(6) = 1,$$
$$y_a(8) = 1,\ y_b(2) = 0,\ y_b(2) = 0,\ y_b(4) = 0, \qquad (20)$$
$$y_b(6) = 0,\ y_b(8) = 0$$

4. Construct the MATLAB code for (19) with (20).

IV. RESULTS AND DISCUSSION

Figure 1 illustrates the velocity profile for the magnetic field *M*. It shows that for increasing values of M, the velocity profile along x-axis is also increasing along the x-axis, while for larger levels of *M*, there is a drop in velocity. The tendency for velocity field values to compress is caused by the larger frictional forces caused by greater *M*. Figure 2 demonstrates how a raise on the magnitude of ϵ causes reduction in velocity. In the physical sense, the rotation rate surpasses the stretching rate as the values increase. When ϵ increases, the fluid encounters more obstacles and experiences greater friction, which hinders its flow and reduces its velocity.

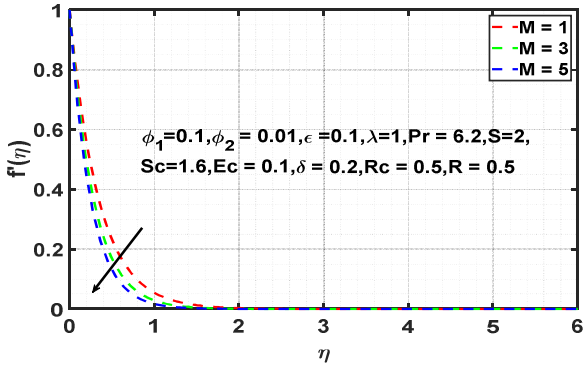

Fig. 1. Effect of *M* on $f'(\eta)$.

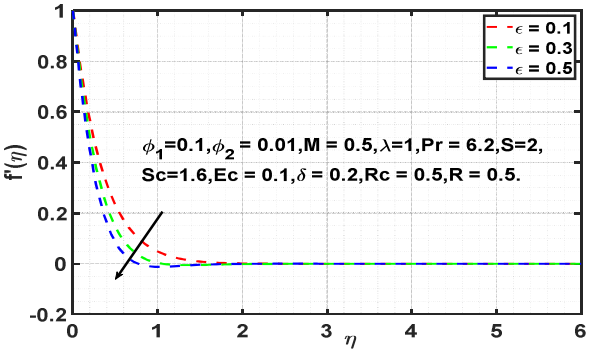

Fig. 2. Effect of ϵ on $f'(\eta)$.

The variations in thermal profiles subject to changes in heat source/sink factor δ are portrayed in Figure 3. The numerical values of δ provide a comparison of the inputs for thermal transmission via conduction and transfer by thermal radiation. Hence, as δ increases, maximum heat diffusion occurs. As a result, the indicated thermal profiles rise with the increased heat source /sink parameter δ. Figure 4 displays that the thermal profile can alter in response to changes in the Eckert number (Ec). Ec is used to measure the impacts of fluid flow that self-heats under the influence of dissipation. As the thermal properties of fluid increase, Ec grows.

In Figure 5, it can be seen that nanoparticle volume fraction is responsible for the diminution in the concentration field associated with a raise in Sc. The concentration regime dwindles with a raise in Sc.

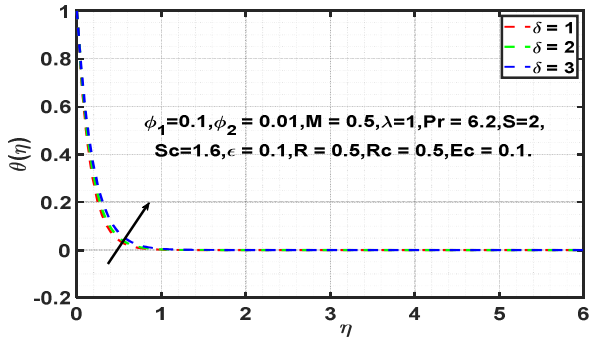

Fig. 3. Effect of δ on $\theta(\eta)$.

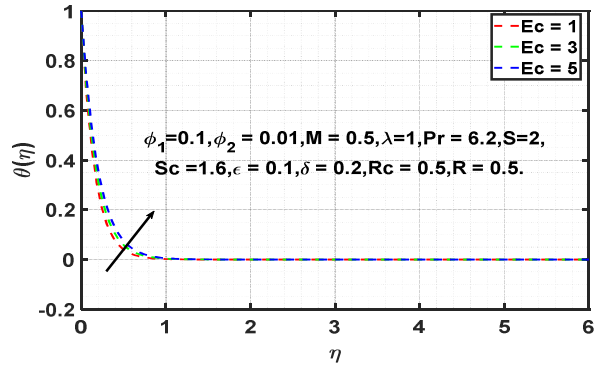

Fig. 4. Effect of Ec on $\theta(\eta)$.

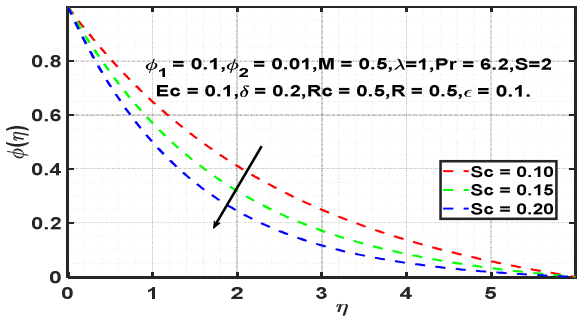

Fig. 5. Effect of Sc on $\phi(\eta)$.

Figures 6-8 exhibit the stretching ratio's $\lambda = b/a$ imprint on the nature of $f'(\eta)$, $\theta(\eta)$, and $\phi(\eta)$. By either raising b along the y-direction or reducing a along the x-direction, the stretching ratio is improved. Figure 6 shows that increasing λ causes the axial velocity $f'(\eta)$ and corresponding layer width to be compressed. Additionally, as the values of λ are raised, the thermal and concentration layer structure deteriorate. Figures 9-11 depict how the suction parameter affects velocity, temperature, and concentration. The tendency of an increase in the suction factor is to force the fluid into an empty area, causing changes on the boundary layer. So, as the suction parameter is increased, velocity slows down. Temperature declines when the suction parameter grows as evidenced in Figure 10. Due to the fluid's inhalation, there is reduced friction between the fluid and the sheet. Hence the heat transfer rate elevates for growing suction values.

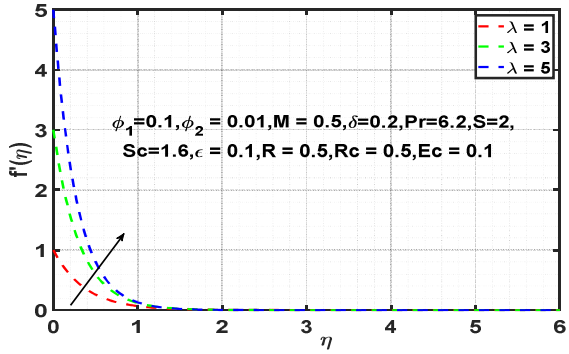

Fig. 6. Effect of λ on $f'(\eta)$.

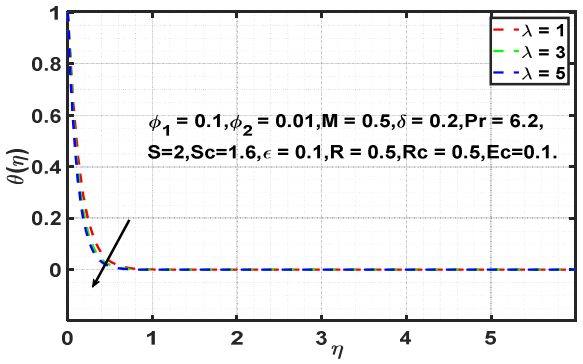

Fig. 7. Effect of λ on $\theta(\eta)$.

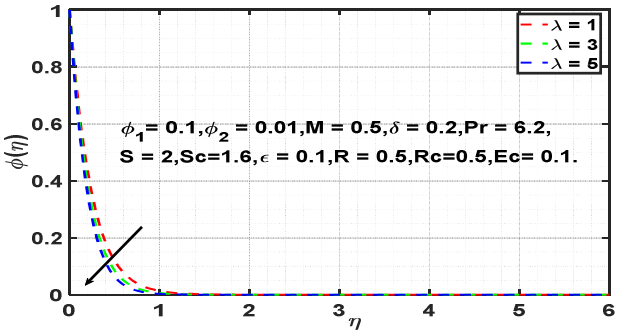

Fig. 8. Effect of λ on $\phi(\eta)$.

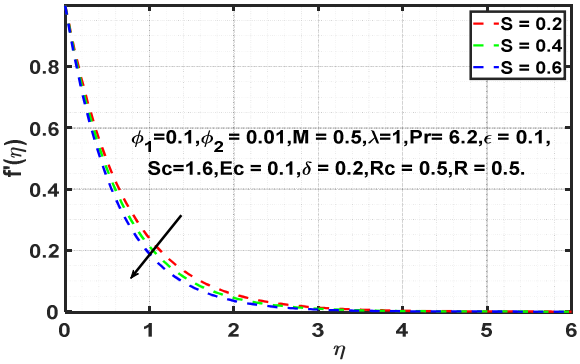

Fig. 9. Effect of S on $f'(\eta)$.

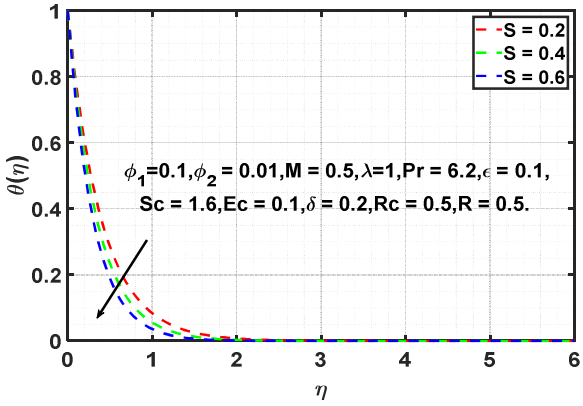

Fig. 10. Effect of S on $\theta(\eta)$.

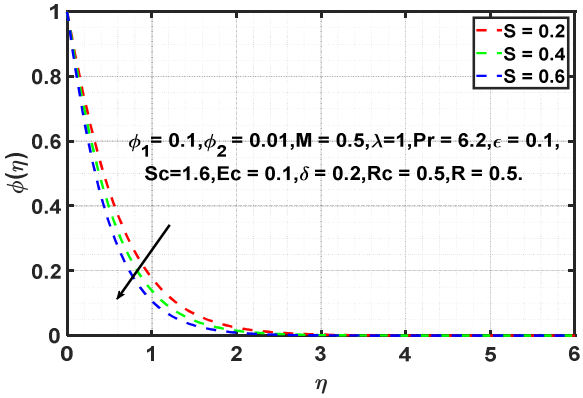

Fig. 11. Effect of S on $\phi(\eta)$.

Figure 12 exhibits the influence of the chemical reaction (Rc) on concentration. Fluid's concentration decreased as the chemical reaction rate increased. Thus the concentration boundary layer thickness improved. In Figure 13, when thermal radiation (R) is present, the heat flow from the sheet rises, changing the temperature distribution and thermal boundary layer thickness. Figure 14 presents the effect of Pr on temperature distribution. Decreasing values of Pr result in a reduction in the temperature dispersion and the related thermal layer thickness.

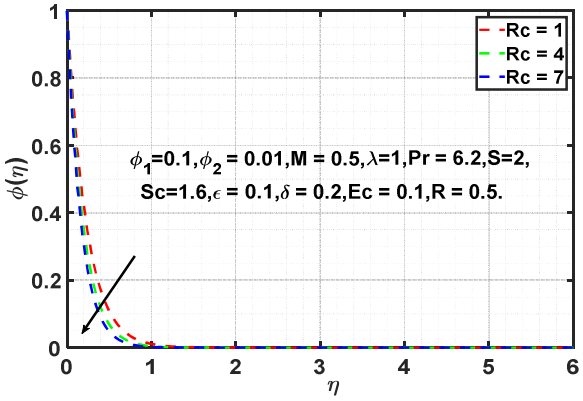

Fig. 12. Effect of Rc on $\phi(\eta)$.

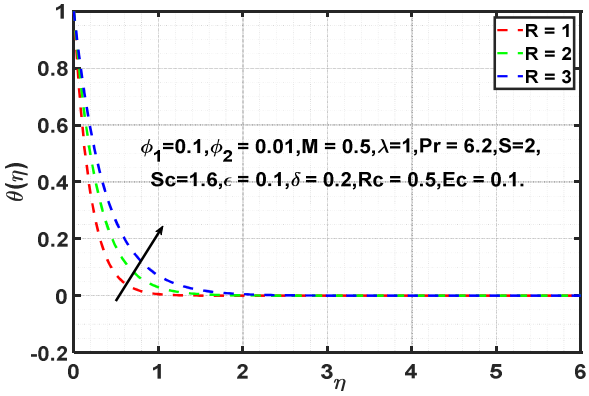

Fig. 13. Effect of R on $\theta(\eta)$.

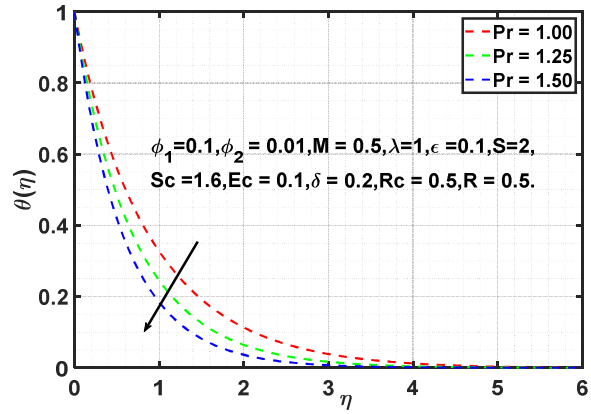

Fig. 14. Effect of Pr on θ.

In Table I, the typical thermophysical characteristics of the HNF are listed, whereas these characteristics' values at 25^0C are provided in Table II. Tables III and IV show the impact for$-f''(0)$, $-g'(0)$, $\theta'(0)$, and $\phi'(0)$. The fixed factor values are: $\phi_1 = 0.1$, $\phi_2 = 0.01$, $\epsilon = 0.1$, $M = 0.5$, $S = 2$, $R = 0.5$, $Sc = 1.6$, $Rc = 0.5$, $\lambda = 1$, $Pr = 6.2$, $Ec = 0.1$, and $\delta = 0.2$.

TABLE I. THERMO PHYSICAL HNF (Al_2O_3-Cu/H_2O) PROPERTIES

Properties	**HNF (Al_2O_3-Cu/H_2O)**
Density ($\boldsymbol{\rho}$)	$\rho_{hnf} = \left((1-\phi_2)\{(1-\phi_1)\rho_f + \phi_1\rho_{s1}\} + \phi_2\rho_{s2}\right)$
Viscosity ($\boldsymbol{\mu}$)	$\mu_{hnf} = \frac{\mu_f}{(1-\phi_1)^{2.5}(1-\phi_2)^{2.5}}$
Heat capacity ($\boldsymbol{\rho C_p}$)	$(\rho C_p)_{hnf} = (1-\phi_2)\left\{(1-\phi_1)(\rho C_p)_f + \phi_1(\rho C_p)_{s1}\right\} + \phi_2(\rho C_p)_{s2}$
Thermal conductivity ($\boldsymbol{K}$)	$\frac{K_{hnf}}{K_{bf}} = \frac{K_{s2} + 2K_{bf} - 2\phi_2(K_{bf} - K_{s2})}{K_{s2} + 2K_{bf} - \phi_2(K_{bf} - K_{s2})}$. where $\frac{K_{bf}}{K_f} = \frac{K_{s1} + 2K_f - 2\phi_1(K_f - K_{s1})}{K_{s1} + 2K_f - \phi_2(K_f - K_{s1})}$
Electrical conductivity (σ)	$\frac{\sigma_{hnf}}{\sigma_{nf}} = \frac{\sigma_{s2} + 2\sigma_{nf} - 2\phi_2(\sigma_{nf} - \sigma_{s2})}{\sigma_{s2} + 2\sigma_{nf} + \phi_2(\sigma_{nf} - \sigma_{s2})}$ where $\frac{\sigma_{nf}}{\sigma_f} = \frac{\sigma_{s1} + 2\sigma_f - 2\phi_1(\sigma_f - \sigma_{s1})}{\sigma_{s1} + 2\sigma_f + \phi_1(\sigma_f - \sigma_{s1})}$.

TABLE II. THERMOPHYSICAL NANOPARTICLE AND BASE FLUID PROPERTIES

Property	**Cu**	**Al_2O_3**	**H_2O**
ρ (kg/m^3)	8933	3987	997.1
C_p (J/kg.k)	385	765	4179
k (W/m.k)	386	40	0.613
σ	3.69x10^7	5.96x10^7	0.05
Pr	-	-	6.20

In Table V, a comparison has been displayed for $f''(0)$, and $g'(0)$ when $\phi_1 = \phi_2 = 0, S = 0, M = 0, Ec = 0.1$, $\lambda = 1$, and $Pr = 6.2$, ignoring volume fractions (ϕ_1, ϕ_2), for stretching rate $\lambda = 1$, at different rotating parameter (ϵ) values.

TABLE III. IMPACT OF $-f''(0)$ ON Al_2O_3-Cu/H_2O HNF

ϕ_1	ϕ_2	S	M	λ	ϵ	$\frac{-1}{(1-\phi_1)^{2.5}(1-\phi_2)^{2.5}} f''(0)$	$\frac{-1}{(1-\phi_1)^{2.5}(1-\phi_2)^{2.5}} g''(0)$
0.1						-3.609131	-0.086696
0.3						-5.454583	-0.149749
0.5						-8.178960	-0.283842
	0.1					-5.253547	-0.115246
	0.4					-11.674354	-0.2941719
	0.5					-14.624638	-0.423901
		0.2				-1.906138	-0.115991
		0.4				-2.059424	-0.114288
		0.6				-2.222998	-0.111901
			1			-3.874919	-0.076656
			2			-4.336035	-0.063932
			3			-4.734578	-0.055964
				1		-3.609131	-0.086696
				3		-12.952087	-0.207714
				5		-24.428558	-0.297522
					0.1	-3.609131	-0.086696
					0.3	-3.622751	-0.258332
					0.5	-3.648707	-0.425087

TABLE IV. IMPACT OF $-\theta'(0), -\phi'(0)$ ON Al_2O_3-Cu/H_2O HNF

ϕ_1	ϕ_2	S	M	Rc	λ	δ	R	ϵ	$-\frac{K_{hnf}}{k_f}\theta'(0)$	$-\frac{K_{hnf}}{k_f}\phi'(0)$
0.1									9.176884	5.515124
0.3									8.755241	6.975468
0.5									8.359225	9.571278
	0.1								9.019446	6.003392
	0.4								8.687348	8.778440
	0.5								8.610743	10.436372
		0.2							3.450877	1.991873
		0.4							3.959441	2.314811
		0.6							4.513250	2.661844
			1						9.111900	5.506764
			2						9.000843	5.493156
			3						8.906460	5.482237
				1					9.176884	5.770677
				4					9.176884	7.016963
				7					9.176884	7.992348
					1				9.176884	5.515124
					3				10.809053	6.042855
					5				11.878708	6.480695
						1			8.703471	5.515124
						2			8.025491	5.515124
						3			7.180675	5.515124
							1		7.066837	5.515124
							2		4.889216	5.515124
							3		3.758518	5.515124
								0.1	9.176884	5.515124
								0.3	9.175439	5.514478
								0.5	9.172680	5.513251

TABLE V. COMPARISON OF THE VALUES OF ϵ FOR $f''(0)$ AND $g'(0)$

	[19]		**[26]**		**Current study**	
ϵ	$f''(0)$	$g'(0)$	$f''(0)$	$g'(0)$	$f''(0)$	$g'(0)$
0	−1	0	−1	0	-1.000484	0.0000
0.5	−1.13838	−0.51276	−1.138374	−0.512760	−1.138479	-0.512684
1.0	−1.32503	−0.83710	−1.325029	−0.837097	−1.325028	-0.837109

V. CONCLUSION

The upper half space $z \geq 0$ of the flow of the Al_2O_3-Cu/H_2O MHD HNF with Rc, R, and δ effects past a permeable, rotating stretching sheet with magnetic regime exhibits a 3-D steady, laminar, Newtonian, and incompressible behavior.

- In response to the increase in magnetic parameter M, HNF's velocity profile rises.
- Velocity $f''(\eta)$, temperature $\theta(\eta)$, concentration $\phi(\eta)$ diminish for increased suction number (S) values.
- When the Eckert number (Ec), Radiation (R), and heat generation/absorption parameter (δ) increase, the thermal boundary layer of HNF AL_2O_3-CU/H_2O also increases.
- With growing values of Sc and Rc, the rate of mass transfer of the surface is enhanced.
- The skin friction coefficients C_{fx}, C_{fy} do not vary with Rc, δ, R. The C_{fx} value diminishes with S, M, and λ.
- The local Nusselt number Nu_x decreases with M, δ, R.
- The Sherwood number S_{hx} increases with Rc, S, λ and decreases with M.

NOMENCLATURE

ϕ_1, ϕ_2 = Volume fractions of the nano particles;
u, v = Velocity components;
a, b = Constants along x-, y-axis;
B = Variable magnetic field;
B_0 = Induced constant magnetic strength;
C_{fx}= Skin friction coefficient along the *x* axis;
C_{fy} = Skin friction coefficient along the *y* axis;
M = Magnetic parameter;
$\epsilon =$ Rotation parameter;
Nux = Nusselt number;
Pr = Prandtl number;
T_∞ = Ambient temperature;
T_w = Surface temperature;
T_0 = Characteristics temperature;
C = Concentration of species;
C_w = Free stream concentration;
C_∞ = Uniform constant concentration;
Re = Reynold's number;
Ec = Eckert number;
Sc = Schimidt number:
bf= Base fluid;
nf= Nano Fluid;
hnf = Hybrid Nano Fluid;
σ_{hnf}= Electrical conductivity of HNF;
μ = Dynamic viscosity;
μ_f = Dynamic viscosity of the fluid;
μ_{hnf} = Viscosity of the HNF;
C_p = Specific heat at constant pressure;
$(\rho Cp)_{hnf}$ = Heat capacity of hybrid nanofluid;
ρ = Density of the fluid;
ρ_{hnf} = Density of the HNF;
K_f = Thermal conductivity of the fluid;
K_{hnf} = Thermal conductivity of HNF;
λ = Stretching/shrinking parameter;
S = Suction parameter;
q_r= Radiation flux;
δ = Heat generation coefficient;
χ = Mean absorption coefficient;
σ = Stefan Boltzmann constant;
Ω = Angular velocity;
ν = Kinematic viscosity;
α_{hnf} = Thermal diffusivities;
β_{hnf}= Concentration diffusivities;
ν_{hnf} = Momentum diffusivities;
S_{hx} = Sherwood number;

REFERENCES

[1] S. Suresh, K. P. Venkitaraj, P. Selvakumar, and M. Chandrasekar, "Synthesis of Al2O3–Cu/water hybrid nanofluids using two step method and its thermo physical properties," *Colloids and Surfaces A: Physicochemical and Engineering Aspects*, vol. 388, no. 1, pp. 41–48, Sep. 2011, https://doi.org/10.1016/j.colsurfa.2011.08.005.

[2] N. A. C. Sidik, I. M. Adamu, M. M. Jamil, G. H. R. Kefayati, R. Mamat, and G. Najafi, "Recent progress on hybrid nanofluids in heat transfer applications: A comprehensive review," *International Communications in Heat and Mass Transfer*, vol. 78, pp. 68–79, Nov. 2016, https://doi.org/10.1016/j.icheatmasstransfer.2016.08.019.

[3] S. U. Devi and S. Devi, "Heat transfer enhancement of Cu-Al2O3/water hybrid nanofluid flow over a stretching sheet," *Journal of the Nigerian Mathematical Society*, vol. 32, no. 2, pp. 419–433, Aug. 2017.

[4] S. S. U. Devi and S. P. A. Devi, "Numerical investigation of three-dimensional hybrid Cu–Al2O3/water nanofluid flow over a stretching sheet with effecting Lorentz force subject to Newtonian heating," *Canadian Journal of Physics*, vol. 94, no. 5, pp. 490–496, May 2016, https://doi.org/10.1139/cjp-2015-0799.

[5] N. S. Khashi'ie, N. M. Arifin, I. Pop, R. Nazar, E. H. Hafidzuddin, and N. Wahi, "Three-Dimensional Hybrid Nanofluid Flow and Heat Transfer past a Permeable Stretching/Shrinking Sheet with Velocity Slip and Convective Condition," *Chinese Journal of Physics*, vol. 66, pp. 157–171, Aug. 2020, https://doi.org/10.1016/j.cjph.2020.03.032.

[6] R. Jusoh, R. Nazar, and I. Pop, "Magnetohydrodynamic rotating flow and heat transfer of ferrofluid due to an exponentially permeable stretching/shrinking sheet," *Journal of Magnetism and Magnetic Materials*, vol. 465, pp. 365–374, Nov. 2018, https://doi.org/10.1016/j.jmmm.2018.06.020.

[7] N. S. Anuar, N. Bachok, N. M. Arifin, H. Rosali, and I. Pop, "Stagnation-Point Flow and Heat Transfer Over an Exponentially Stretching/Shrinking Sheet in Hybrid Nanofluid with Slip Velocity Effect: Stability Analysis," *Journal of Physics: Conference Series*, vol. 1366, Nov. 2019, Art. no. 012002, https://doi.org/10.1088/1742-6596/1366/1/012002.

[8] I. Waini, A. Ishak, and I. Pop, "Unsteady flow and heat transfer past a stretching/shrinking sheet in a hybrid nanofluid," *International Journal of Heat and Mass Transfer*, vol. 136, pp. 288–297, Jun. 2019, https://doi.org/10.1016/j.ijheatmasstransfer.2019.02.101.

[9] I. Waini, A. Ishak, and I. Pop, "Flow and heat transfer along a permeable stretching/shrinking curved surface in a hybrid nanofluid," *Physica Scripta*, vol. 94, no. 10, Oct. 2019, Art. no. 105219, https://doi.org/10.1088/1402-4896/ab0fd5.

[10] I. Waini, A. Ishak, and I. Pop, "Hybrid nanofluid flow and heat transfer over a nonlinear permeable stretching/shrinking surface," *International Journal of Numerical Methods for Heat & Fluid Flow*, vol. 29, no. 9, pp. 3110–3127, Jan. 2019, https://doi.org/10.1108/HFF-01-2019-0057.

[11] N. S. Khashi'ie, N. M. Arifin, R. Nazar, E. H. Hafidzuddin, N. Wahi, and I. Pop, "Magnetohydrodynamics (MHD) axisymmetric flow and heat transfer of a hybrid nanofluid past a radially permeable stretching/shrinking sheet with Joule heating," *Chinese Journal of Physics*, vol. 64, pp. 251–263, Apr. 2020, https://doi.org/10.1016/j.cjph.2019.11.008.

[12] N. C. Rosca, A. V. Rosca, and I. Pop, "Axisymmetric flow of hybrid nanofluid due to a permeable non-linearly stretching/shrinking sheet with radiation effect," *International Journal of Numerical Methods for Heat & Fluid Flow*, vol. 31, no. 7, pp. 2330–2346, Jan. 2020, https://doi.org/10.1108/HFF-09-2020-0574.

[13] M. Shoaib *et al.*, "Numerical investigation for rotating flow of MHD hybrid nanofluid with thermal radiation over a stretching sheet," *Scientific Reports*, vol. 10, no. 1, Oct. 2020, Art. no. 18533, https://doi.org/10.1038/s41598-020-75254-8.

[14] A. Asghar, L. A. Lund, Z. Shah, N. Vrinceanu, W. Deebani, and M. Shutaywi, "Effect of Thermal Radiation on Three-Dimensional Magnetized Rotating Flow of a Hybrid Nanofluid," *Nanomaterials*, vol. 12, no. 9, Jan. 2022, Art. no. 1566, https://doi.org/10.3390/nano12091566.

[15] N. F. H. Mohd Sohut, S. K. Soid, S. Abu Bakar, and A. Ishak, "Unsteady Three-Dimensional Flow in a Rotating Hybrid Nanofluid over a Stretching Sheet," *Mathematics*, vol. 10, no. 3, Jan. 2022, Art. no. 348, https://doi.org/10.3390/math10030348.

[16] U. Farooq, M. Tahir, H. Waqas, T. Muhammad, A. Alshehri, and M. Imran, "Investigation of 3D flow of magnetized hybrid nanofluid with heat source/sink over a stretching sheet," *Scientific Reports*, vol. 12, no. 1, Jul. 2022, Art. no. 12254, https://doi.org/10.1038/s41598-022-15658-w.

[17] A. Jaafar, I. Waini, A. Jamaludin, R. Nazar, and I. Pop, "MHD flow and heat transfer of a hybrid nanofluid past a nonlinear surface stretching/shrinking with effects of thermal radiation and suction," *Chinese Journal of Physics*, vol. 79, pp. 13–27, Oct. 2022, https://doi.org/10.1016/j.cjph.2022.06.026.

[18] K. Boukerma and M. Kadja, "Convective Heat Transfer of Al2O3 and CuO Nanofluids Using Various Mixtures of Water-Ethylene Glycol as Base Fluids," *Engineering, Technology & Applied Science Research*, vol. 7, no. 2, pp. 1496–1503, Apr. 2017, https://doi.org/10.48084/etasr.1051.

[19] N. S. Anuar, N. Bachok, and I. Pop, "Radiative hybrid nanofluid flow past a rotating permeable stretching/shrinking sheet," *International Journal of Numerical Methods for Heat & Fluid Flow*, vol. 31, no. 3, pp. 914–932, Jan. 2020, https://doi.org/10.1108/HFF-03-2020-0149.

[20] T. Hayat and S. Nadeem, "Heat transfer enhancement with Ag–CuO/water hybrid nanofluid," *Results in Physics*, vol. 7, pp. 2317–2324, Jan. 2017, https://doi.org/10.1016/j.rinp.2017.06.034.

[21] T. Hayat, S. Nadeem, and A. U. Khan, "Rotating flow of Ag-CuO/H2O hybrid nanofluid with radiation and partial slip boundary effects," *The European Physical Journal E*, vol. 41, no. 6, Jun. 2018, Art. no. 75, https://doi.org/10.1140/epje/i2018-11682-y.

[22] C. Maheswari, R. Ramana, S. Shaw, D. Gurram, and S. Noeiaghdam, "Numerical investigation on MHD forchheimer flow of Fe3O4-H2O, Cu-H2O and Ag-H2O nanofluids over permeable stretching sheet with radiation," *Results in Engineering*, vol. 18, Jun. 2023, Art. no. 101194, https://doi.org/10.1016/j.rineng.2023.101194.

[23] G. Dharmaiah, R. M. Ramana, Sk. M. Shaw, and N. Dasari, "Effect of nanoparticle volume fraction on MHD water based nanofluid flows over a permeable stretching sheet with suction/injection," *AIP Conference Proceedings*, vol. 2699, no. 1, Jun. 2023, Art. no. 020028, https://doi.org/10.1063/5.0139888.

[24] R. Mohana Ramana, K. Venkateswara Raju, and J. Girish Kumar, "Multiple slips and heat source effects on MHD stagnation point flow of casson fluid over a stretching sheet in the presence of chemical reaction," *Materials Today: Proceedings*, vol. 49, pp. 2306–2315, Jan. 2022, https://doi.org/10.1016/j.matpr.2021.09.348.

[25] H. B. Lanjwani, M. S. Chandio, K. Malik, and M. M. Shaikh, "Stability Analysis of Boundary Layer Flow and Heat Transfer of Fe2O3 and Fe-Water Base Nanofluid over a Stretching/Shrinking Sheet with Radiation Effect," *Engineering, Technology & Applied Science Research*, vol. 12, no. 1, pp. 8114–8122, Feb. 2022, https://doi.org/10.48084/etasr.4649.

[26] Y. Y. Teh and A. Ashgar, "Three Dimensional MHD Hybrid Nanofluid Flow with Rotating Stretching/Shrinking Sheet and Joule Heating," *CFD Letters*, vol. 13, no. 8, pp. 1–19, Aug. 2021, https://doi.org/10.37934/cfdl.13.8.119.